Available online at www.sciencedirect.com
SCIENCE DIRECT®

Journal of the European Ceramic Society 24 (2004) 619–626

www.elsevier.com/locate/jeurceramsoc

Comparison of fracture surface and plane section analysis for ceramic grain size characterisation

A.L. Horovistiz[a,*], J.R. Frade[b], L.R.O. Hein[a]

[a]*Universidade Estadual Paulista "Júlio de Mesquita Filho", Departamento de Materiais Tecnologia, Av. Ariberto Pereira da Cunha 333, Pedregulho, 12516-410, Guaratinguetá, SP, Brazil*

[b]*Universidade de Aveiro,Campus Universitário de Santiago, Departamento de Engenharia Cerâmica e do Vidro, 3810-193 Aveiro, Portugal*

Received 2 November 2002; received in revised form 10 March 2003; accepted 6 April 2003

Abstract

A method has been developed to obtain quantitative information about grain size and shape from fractured surfaces of ceramic materials. One elaborated a routine to split intergranular and transgranular grains facets of ceramic fracture surfaces by digital image processing. A commercial ceramic (ALCOA A-16, Al_2O_3–1.5% of CrO) was used to test the proposed method. Microstructural measurements of grain shape and size taken from fracture surfaces have been compared through descriptive statistics of distributions, with the corresponding measurements from polished and etched surfaces. The agreement between results, with the expected bias on grain size values from fractures, obtained for both types of surfaces allowed to infer that this new technique can be used to extract the relevant microstructural information from fractured surfaces, thus minimising the time consuming steps of sample preparation.

Keywords: Grain size; Microstructure-final; Fracture; Al_2O_3; Digital image processing

1. Introduction and objectives

Information on microstructural features of ceramic materials is essential to select suitable sintering conditions, to optimise their thermo-mechanical performance, to suppress negative effects of microstructural defects on relevant properties, and/or to design optimised microstructural features for prospective applications. These relationships are most obvious in the field of electroceramics, and ceramics with strict thermo-mechanical requirements. Typical examples include sintering at relatively low temperatures to prevent high temperature degradation, to enhance the mechanical properties by retaining sub-micrometer grain sizes,[1] or to explore unique properties of nanomaterials. Other examples refer to important grain boundary controlled properties of different types of electroceramics,[2–6] and the widely recognised blocking effects of grain boundaries in most ionic conductors.[7–10] The dependence of electrical properties on microstructural features of ceramic materials is also the basis of methods proposed to monitor the sintering behaviour by electrical measurements.[11]

Some important properties of ceramic materials may be dependent not only on porosity and microstructural features such as the grain size and/or pore size distributions, grain shape and its distribution. A demonstration of the role of grain shape on the electrical behaviour was reported in the literature.[4]

The development of advanced ceramic materials and the widely recognised intrinsic relationship between their properties and microstructure must thus rely on robust and trustworthy microstructural analysis techniques; this is based on quantitative microscopy, supported by digital image processing and stereology. Its development has relied on hardware evolution and the availability of software for digital image processing and analysis.

Several works[1–5] have reported methods to extract microstructural information from the polished and etched surfaces of ceramic materials obtained through quantitative microscopy. This approach has many advantages, when compared to other methods, such as

* Corresponding author.
E-mail address: horovistiz@cv.ua.pt (A.L. Horovistiz).

0955-2219/03/$ - see front matter © 2003 Elsevier Ltd. All rights reserved.
doi:10.1016/S0955-2219(03)00260-7

reducing the data acquisition time, improving the accuracy and reproducibility, and a perfect linking to new concepts of digital microscopy. However, ceramographic procedures are often very tedious and time consuming, sometimes changing the original microstructures, or failing to yield the desired results.[6–23] Alternatively, quantitative information about size of ceramic grains could be obtained by the analysis of fracture surfaces of bulk samples, without using time consuming ceramographic procedures. Fracture surfaces are not random compared to microstructure but it is acceptable that the intergranular facets exposed by the fracture process are dependent on grain size. Thus, the significance of quantitative information about grain size measured from fracture surfaces must be checked from a statistical point of view, to evaluate the bias due to the restriction imposed by intergranular facets.

Ceramic materials present mainly brittle fracture[24] and the crack path can be intergranular or transgranular. Detection of grain boundaries is easy in the case of intergranular fracture but might be very difficult in the case of transgranular fracture. In addition, the fracture surface shows an irregular trajectory of grain facets and its observation by scanning electron microscope (SEM) often yields acquired images with poor contrast and saturation on contours.[25] These difficulties thus limit the usefulness of this approach.

The goal of the present work is to propose a method of microstructural characterisation from fractured surfaces as an alternative to inspection of polished surfaces. The method is based on the routines of a public domain digital image processing program: the NIH Image J.[1] This approach consists of the following steps: (1) to elaborate a routine to split intergranular and transgranular grains facets of ceramic fracture surfaces by digital image processing, (2) to obtain grain size measurements from fracture surfaces, (3) to compare these data against grain size measurements from the corresponding polished and etched surface of the same ceramic, to check the method validation.

2. Materials

The starting materials were commercially available Al_2O_3 (A-16 ALCOA, USA) and Cr_2O_3 (Carlo Erba, Italy). An amount of 200 g of composition (1.5% of Cr_2O_3) was put in a laboratory ball mill, together with 70 ml of water and alumina balls mill as milling media. They were then milled for 48 h, followed by drying of slurry at 100 °C. The as-dried powder mixture was ground using an alumina mortar and pestle, to eliminate large powder agglomerates, and then passed through 60-mesh sieves. After grained it was uniaxial pressed, it was used a steel mould with 65×65 mm and the stress was 50 MPa. The plates obtained were sintered at 1600 °C.

Samples for fracture surface analysis and for conventional ceramographic quantitative analysis were taken from the same bulk ceramic plate. One of these subsamples was polished and thermally etched at 1350 °C, during 30 min, to reveal the grain boundaries, as recommended in the literature.[26] This sample was observed by reflective light microscopy. Ballistic testing of another sub-sample produced fracture surfaces. This fracture surface was observed by scanning electron microscopy (SEM), with 10 kV beam voltage and using the secondary electron detector. This sampling intends to reduce differences on grain size distribution for better comparison between the conventional observation of polished surfaces, and the present method proposed to characterise the grain size and shape based on fracture surfaces.

3. Image processing

The selection of light contrast and image processing used for polished and etched surfaces was performed as follows:

1. The boundaries of grains or pores were enhanced by improving the image contrast, e.g. increasing the brightness differences between neighbour regions, as proposed elsewhere.[27] Both brightfield illumination and DIC (differential interference contrast) Nomarsky with green intensity filters were used in order to optimise the images (Fig. 1a).
2. Background removal (or shading correction) was used to attain the same glare or shading distribution at different picture region.[28] In this work, a 15×15 mean filter was carried out on the original image to find the shading background; this was subtracted from the original image, pixel by pixel.
3. Linear histogram equalisation was then applied to generate uniform brightness distribution. A 3×3 median filter was applied in order to reduce the effect of saturated points on images due to the noise from digital acquisition[29](Fig. 1b). After this step, the brightness histogram presents a bimodal distribution and the thresholding for image binarisation is easily performed by selecting the grey-level at the minimum valley between the two mode peaks. The contours are now well defined, but some noise points and small false objects are still present inside grains and could distort the results for pore analysis. Again, the use of a 3×3 median filter can reduce or eliminate these features (Fig. 1c).

[1] NIH Image J public domain program is conducted by Wayne Rasband from the National Institutes of Health (http://rsb.info.nih.gov/ij).

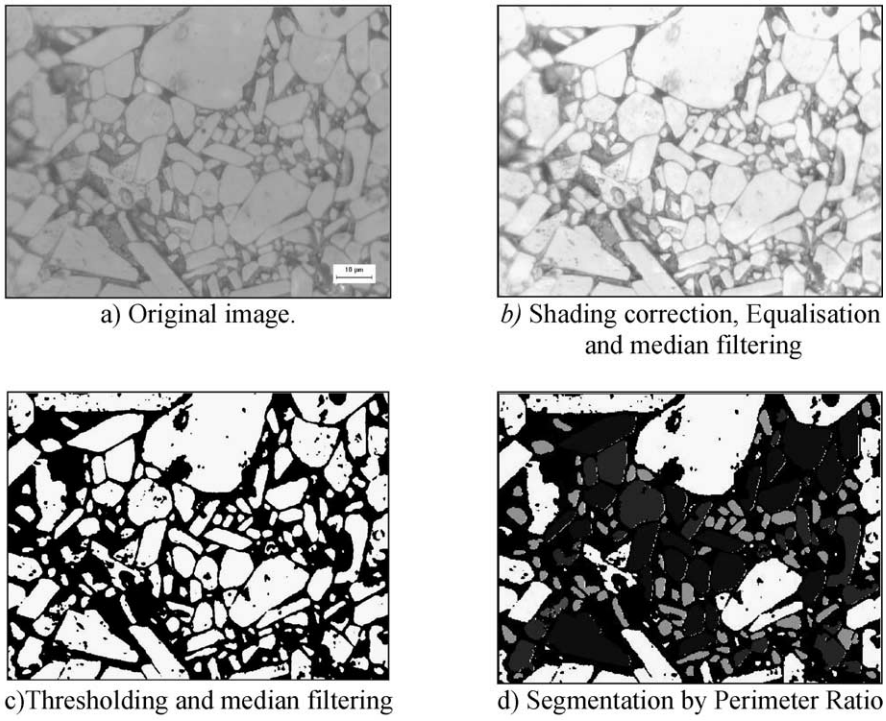

Fig. 1. Sequence for digital image processing for polished and etched surface: (a) original image; (b) shading correction, equalisation and median filtering; (c) thresholding and median filtering; (d) segmentation by perimeter ratio.

The selected parameter for shape segmentation is the perimeter ratio (PR) defined as follows:

$$\mathrm{PR} = \frac{P_{\mathrm{cv}}}{P_{\mathrm{cc}}} \tag{1}$$

where P_{cc} is the concave (or true) perimeter of the object, P_{cv} is the convex perimeter. This perimeter ratio is sensitive to identify the breakouts and grains connected by apparent (ghost) boundaries. Sample preparation conditions such as compressive moulding and sintering processes should not change so much the convex form of original particles. The definition of PR range was experimentally determined, by checking PR values in a subset of sampling fields, defining the tolerated degree of concavity and excluding the effects of ghost boundaries and breakouts. In this case, only grains presenting PR values inside the range from 0.90 to 1.00 were considered for image analysis. One also avoided counting the grains at image borders (Fig. 1d).

The first problem encountered on the digital image processing of the grains from fracture surface was the irregular *shading*, which disturbs the image on analysis (Fig 2a). Thus, a background removal filter was used. In order to correct the low contrast, the histogram equalisation was applied, as this operation preserved approximately all the details of grain boundaries[30] (Fig. 2b).

The next step of digital image processing was the separation of intergranular fraction and transgranular fraction, to be able to exclude transgranular fracture regions. Note that one can not delimit grains on transgranular regions, due to hidden boundaries and rougher texture on fracture surface, which can produce false grain limits. Detection of poorly contrasted intergranular grain boundaries is also troublesome. From this step, two different image processing methods applied to the same image were performed after image duplication. A 3×3 median filter was applied to one of the duplicated images, to eliminate some saturated points (pixels with very different brightness from neighbour regions) (Fig. 2c). The copy image was treated with a *high-pass convolution filter*, using a kernel 3×3, such as:

$$\begin{bmatrix} -1 & -1 & -1 \\ -1 & +12 & -1 \\ -1 & -1 & -1 \end{bmatrix} \tag{2}$$

This increases the high-frequency information (sharpening edges),[31] but it also yields somewhat noisier images (Fig. 2d).

From the smoothed image, one opted for decomposition of image into waviness and roughness followed by application of a Gaussian filter. The waviness component corresponds to long wavelengths (or low frequency) from the original image, while the roughness component correspond to short wavelengths (or high frequency) of the original surface.[32] The effect of this

operation allows to distinguishing the intergranular fracture surface (roughness) (Fig. 2e) and transgranular fracture surface (waviness) (Fig. 2f) from the original image.

From the roughness image a thresholding for image binarisation was performed (Fig. 2g), while a first-order variance operator was applied on the sharper image. This filter was selected because it reveals just one border at grain boundaries instead of two borders, as for the most popular approaches of edge detection filters, such as Sobel or Roberts derivative filters, based on the derivative function (second-order operators). The next step was a thresholding for image binarisation (Fig. 2h), and contours are defined after an average between both images (Fig. 2g and 2h). This operation offers the advantage of keeping the boundaries while smoothing the noise. This is shown in Fig. 2i, after binarisation.

A set of binary mathematical morphological operations was applied in order to close grain boundaries; this was a two step procedure, consisting of a dilation operation,

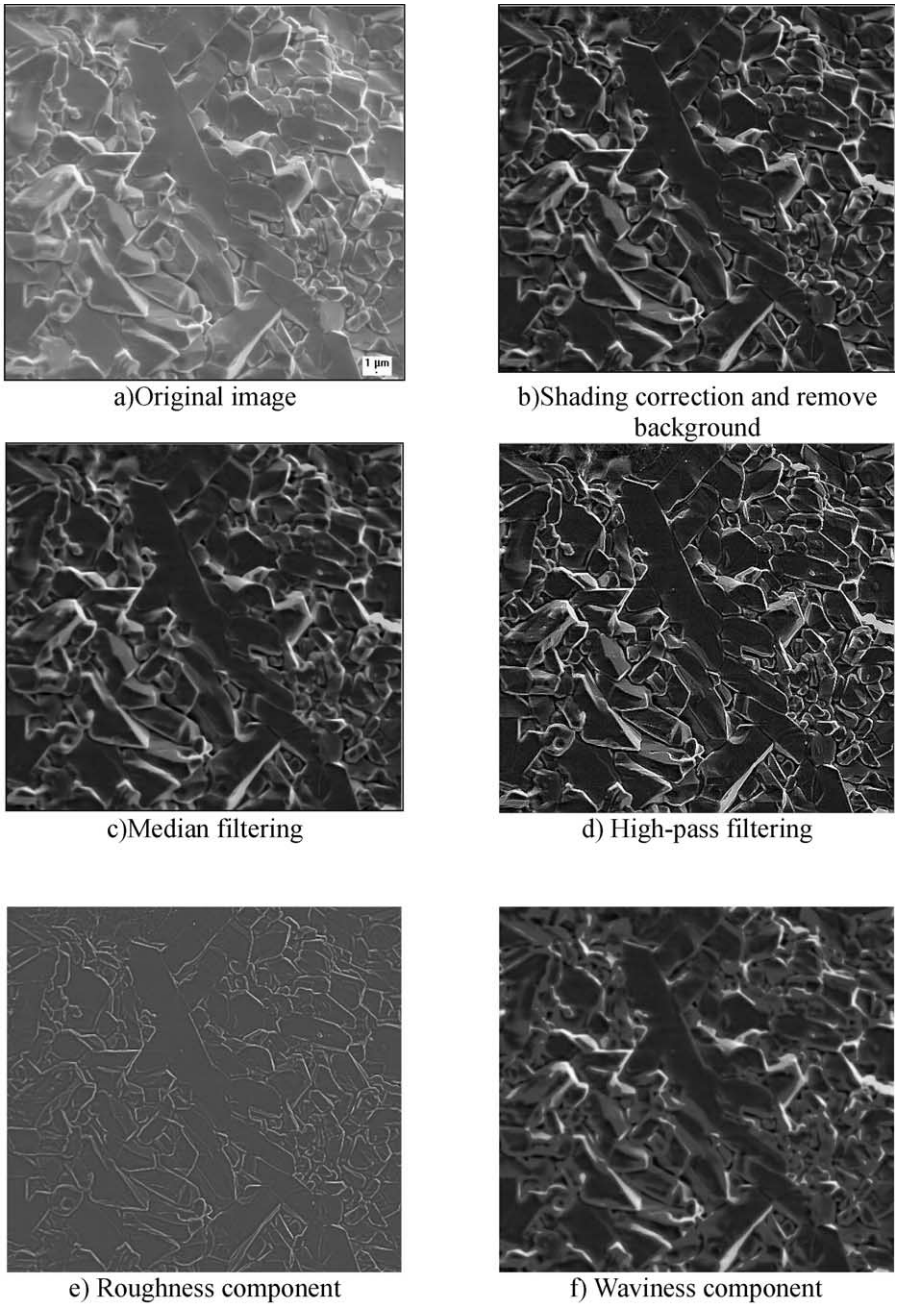

Fig. 2. Sequence of digital image processing for fractured surface: (a) original image; (b) shading correction and remove background; (c) median filtering; (d) high-pass filtering; (e) roughness component; (f) waviness component; (g) thresholding; (h) variance filtering and thresholding; (i) average between g and h, median filtering and binarisation; (j) amplification of transgranular region; (k) dilation operation; (l) skeletonisation operation; (m) segmentation by perimeter ratio; (n) Comparison with the original image.

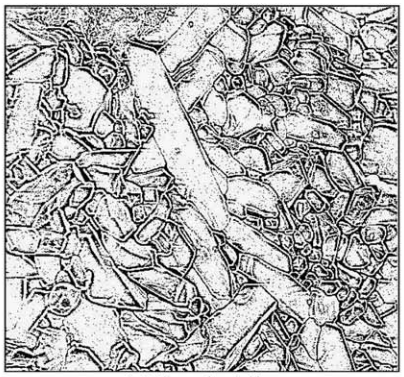

g) Thresholding

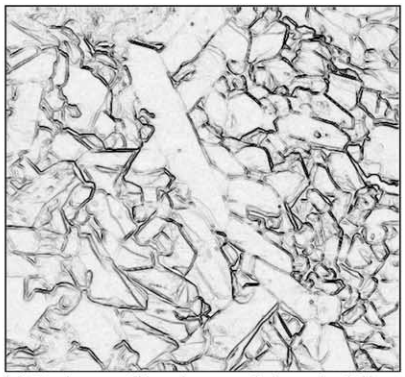

h)Variance filtering and thresholding

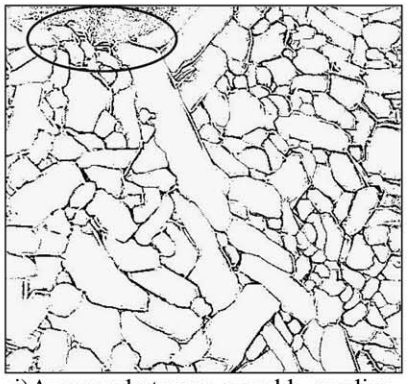

i)Average between g and h, median filtering and binarisation

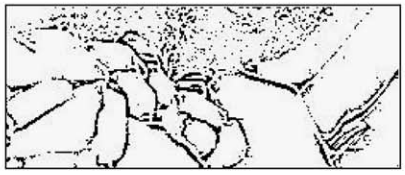

j) Amplification of transgranular region from Fig 2i

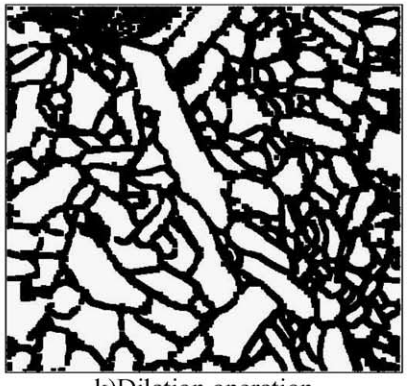

k)Dilation operation

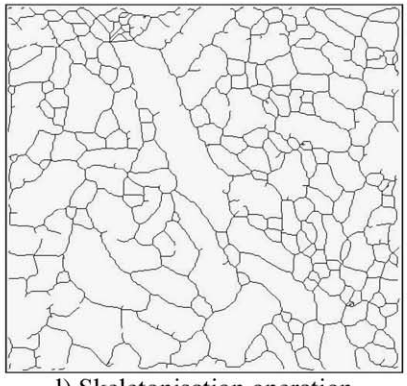

l) Skeletonisation operation

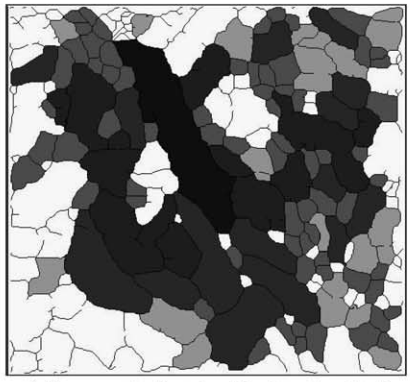

m) Segmentation by Perimeter Ratio

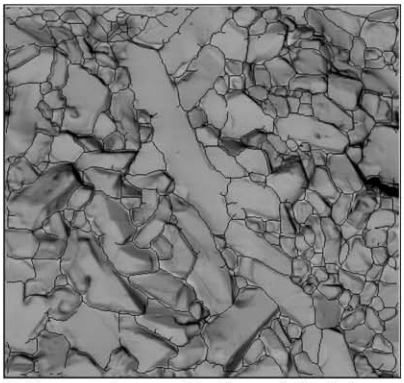

n) Comparison with the original image

Fig. 2. (*continued*).

whose net effect is to expand the shapes in the input image[34] (Fig. 2j), followed by skeletonisation that preserves the main properties of the original image (Fig. 2k).

The parameter for shape segmentation, i.e. the perimeter ratio (PR), was applied on fractured surfaces and the range of values were the same (Fig. 2l). A comparison with the original image is showed in Fig. 2m.

A critical step of image processing was the selection of suitable parameters for the dilation operation. The decision about the number of dilation cycles and their coefficients of neighbouring was empirical in order to ensure that intergranular grains are shown closed, mainly to keep the misshapen transgranular fraction that has been destroyed by the roughness/waviness plug-in application (Fig. 2j). This strategy is somewhat hazardous due to over segmentation that can be caused by classical dilation with the 3×3 cross structuring element adopted by NIH Image J.

To minimise this effect, the shape segmentation by the perimeter ratio (Fig. 2l) was adopted to exclude false grains generated by over segmentation, which mainly occur at transgranular regions. In fact, the option for the combination of skeletonisation followed by shape segmentation, instead of the watershed method after dilation is more effective for grain identification.[33]

Watershed algorithms often add false boundaries for irregular grains or those grains with changes in width. So, watershed method was not applied due its tendency to reduce the mean grain size, due to over segmentation on grains with some degree of concavity.

4. Analysis

In spite of the fact that this method has been developed for ceramics whose fracture is mainly intergranular,[34,35] this approach may be valid also for ceramic materials with a predominant transgranular fraction, provided that the transgranular surface has some image texture variation to be able to detect component waviness of the decomposition operation; this condition was met in the present study. Otherwise, if the transgranular fraction is smooth, one takes a risk to add a large quantity of false grains to the measurement. An efficient and elegant way to solve this problem is the adoption of the median value as an analytical parameter, since it can filter the outlier measures.[36,37]

The following parameters to evaluate grain morphology were chosen:

1. Grain area
2. Mean diameter
3. Roundness, to evaluate grains shape
4. Aspect ratio, or the ratio between maximum and minimum chord lengths inside an object to evaluate the grain morphology

Table 1 summarises and compares the statistical results obtained for grains from one polished sub-sample and grains of one fractured sub-sample. The descriptive statistics that include the coefficient of variation[38] was applied in the present study. The *rank sum test* was used in order to compare the distributions obtained for polished surface and for fracture surfaces. Note that the populations do not have normal distribution. This statistical test was used to determine if there is a significant difference between two groups, i.e. to check if this is greater than expected for random sampling variation. Populations of about 1000 grains were analysed as indicated elsewhere.[39]

Size measurements of fractured grains tend to be smaller than the size measurement of polished grains, and Table 1 shows a difference of about 7% between the mean of diameters of the populations of polished grains and fractured grains. The values of aspect ratio are also systematically smaller for fractured grains than for polished grains. This may be due to stereological sampling, because grain geometry is always investigated from sections. In the case of the polished surface, the section cut is oriented and positioned randomly, so that 2D sections of grains differ in their shape and size, depending on the geometry of grains and on distance of the cut plane from the grain centre. Some models were proposed in the literature to describe the distribution functions of shape and size parameters in polycrystalline samples, and to explain the effects of grain shape on these distributions.[40] On fracture surfaces of predominant intergranular character, the crack path often

Table 1
Comparative data to morphology and size measurements from descriptive statistics of distributions

Parameters		Grains from polished and etched surface	Grains from fractured surface
Area	*Mean*	18.144	15.344
	Median	9.26	8.72
	Standard deviation	36.576	34.857
	Coefficient of variation	*2.015*	*2.032*
Aspect ratio	*Mean*	2.068	1.986
	Median	1.886	1.822
	Standard deviation	0.791	0.646
	Coefficient of variation	*0.382*	*0.325*
Mean Diameter	*Mean*	4.748	4.42
	Median	3.430	3.326
	Standard deviation	3.786	3.297
	Coefficient of variation	*0.797*	*0.757*

follows irregular sequence of grain facets, and grain facets are often shown smaller than randomly oriented sections. Thus, the size and shape distributions will be systematically smaller for fracture surfaces than for the corresponding polished surfaces; but both procedures lead to similar distributions.

5. Conclusions

The present results and analysis suggest that the proposed method can be used to obtain microstructural information from fractured surface of ceramics; this represents time economy by avoiding, or at least minimising the polishing and etching steps of ceramographic procedures. The size and shape measures obtained for fracture surfaces were closer than those obtained from polished and etched surfaces, but biased for lower values, as expected. It is important to notice that all size or shape distributions presented the same tendencies and were considered similar by rank sum test. The differences between results obtained for fracture surfaces and polished surfaces are systematic and can be rationalised by taking into account that the transgranular fracture is not entirely random for grains with a relatively large aspect ratio. It is certainly necessary to compare the size and shape distributions for fracture and polished surfaces of many other ceramic systems to validate the method. However, since verifying the systematic bias, we confide that such results will provide more compelling evidence, and that microstructural analysis from fracture surfaces will find widespread utilisation.

Acknowledgements

The authors would like to acknowledge to Dr. Francisco Cristovão Lourenço de Melo of CTA, Dr. Elson de Campos and Dr. Flávio de Paula Santos of EEAer for helpful comments.

The results presented in this paper were obtained in framework of the works on project No. 2001/09664-1 supported by FAPESP (Fundação de Amparo à Pesquisa do Estado de São Paulo).

References

1. Kleinlogel, C. M. and Gaukler, L. J., Sintering and properties of nanosized ceria solid solutions. *Solid State Ionics*, 2000, **245**, 567–573.
2. Yamaoka, N. and Matsui, T., Properties of SrTiO3-based boundary layer capacitors. In *Advances in Ceramics, Vol. I, Grain Boundary Phenomena in Electronic Ceramics*, ed. L. M. Levinson and D. C. Hill. American Ceramic Society, Columbus, OH, 1981, pp. 232–241.
3. Denk, I., Claus, J. and Maier, J., Electrochemical investigations of $SrTiO_3$ boundaries. *J. Electrochem. Soc.*, 1997, **144**, 3526–3535.
4. Fleig, J. and Maier, J., A finite element study on the grain boundary impedance of different microstructures. *J. Electrochem. Soc.*, 1998, **145**, 2081–2089.
5. Abrantes, J. C. C., Labrincha, J. A. and Frade, J. R., Applicability of the brick layer model to describe the grain boundary properties of strontium titanate ceramics. *J. Eur. Ceram. Soc.*, 2000, **20**, 1603–1609.
6. Abrantes, J. C. C., Labrincha, J. A. and Frade, J. R., Behaviour of strontium titanate ceramics in reducing conditions suggesting enhanced conductivity along grain contacts. *J. Eur. Ceram. Soc.*, 2002, **22**, 1683–1691.
7. Van Dijk, T. and Burggraaf, A. J., Grain boundary effects on ionic conductivity in ceramic $Gd_xZr_{1-x}O_{2-x/2}$ solid solutions. *Phys. Stat. Sol. A*, 1981, **63**, 229–240.
8. Boutz, M. M. R., Chen, C. S., Winnubst, L. and Burggraaf, A. J., Characterisation of grain boundaries in superplastically deformed Y-TZP ceramics. *J. Amer. Ceram. Soc.*, 1994, **77**, 632–640.
9. Santos, P., Domingues, R. Z. and Kleitz, M., Grain boundary blocking effect in tetragonal yttria stabilised zirconia. *J. Eur. Ceram. Soc.*, 1998, **18**, 1571–1579.
10. Christie, G. M. and van Berkel, F. P. F., Microstructure—ionic conductivity relationships in ceria-gadolinia electrolytes. *Solid State Ionics*, 1996, **83**, 17–27.
11. Steil, M. C., Thevenot, F. and Kleitz, M., Densification of yttria stabilised zirconia: Impedance spectroscopy analysis. *J. Electrochem. Soc.*, 1997, **144**, 390–398.
12. Cwajna, J., Chraponski, J. and Malinski, M., Grain size description—relationships between 2D and 3D parameters. *Acta Stereol*, 1999, **18**, 61–66.
13. Richter, J., Cwajna, J. and Szala, J., Evaluation of sintered carbides microstructure through automatic image analysis. *Acta Stereol*, 1999, **18**, 67–74.
14. Szala, J. and Cwajna, J., Image analysis of polycrystalline materials microstructure. *Acta Stereol*, 1999, **18**, 89–94.
15. Coster, M. and Chermant, J. L., Trends and challenges in the morphological study of ceramics. *Acta Stereol*, 1999, **18**, 283–296.
16. Mitic, V. V., Nikolic, Z. S., Mitrovic, I., Jordovic, B. and Brankov, V., The application of sterology method for estimating the number of 3D $BaTiO_3$-ceramic grains contact surface. *Image Anal. Stereol*, 2001, **20**, 231–277.
17. Carle, V. M., Schafer, U., Taffner, U., Predel, F., Telle, R. and Petzow, G., Ceramographic of high performance ceramics description of materials, preparation, etching techniques and description of microstructures—Part I: ceramografic etching. *Prakt. Met*, 1991, **28**, 359–376.
18. Carle, V. M., Schafer, U., Taffner, U., Predel, F., Telle, R. and Petzow, G., Ceramographic of high performance ceramics description of materials, preparation, etching techniques and description of microstructures—Part II: Silicon carbides. *Prakt. Met*, 1991, **28**, 421–434.
19. Schafer, U., Schubert, H., Carle, V. M., Taffner, U., Predel, F. and Petzow, G., Ceramographic of high performance ceramics description of materials, preparation, etching techniques and description of microstructures—Part III: zirconium dioxide (ZrO_2). *Prakt. Met*, 1991, **28**, 469–482.
20. Predel, F., Bazin, J. P., Carle, V. M., Schafer, U., Schubert, H., Taffner, U., Telle, R. and Petzow, G., Ceramographic of high performance ceramics description of materials, preparation, etching techniques and description of microstructures—Part IV: aluminum nitride. *Prakt. Met*, 1991, **28**, 543–552.
21. Taffner, U., Carle, V. M., Schafer, U., Predel, F. and Petzow, G., Ceramographic of high performance ceramics description of materials, preparation, etching techniques and description of microstructures—Part V: silicon nitride(Si_3N_4). *Prakt. Met*, 1991, **28**, 593–610.
22. Taffner, U., Jaeger, H., Carle, V. M., Taffner, U., Predel, F. and Petzow, G., Ceramographic of high performance ceramics

description of materials, preparation, etching techniques and description of microstructures—Part VI: high-temperature superconductor $YBa_2Cu_3O_7$. *Prakt. Met*, 1991, **28**, 633–648.
23. Carle, V. M., Trippel, B., Taffner, U., Jaeger, H., Taffner, U., Schafer, U., Predel, F., Telle, R. and Petzow, G., Ceramographic of high performance ceramics description of materials, preparation, etching techniques and description of microstructures—Part VIII: aluminium oxide(Al_2O_3). *Prakt. Met*, 1991, **28**, 55–76.
24. Hull, D., *Fractography: Observing, measuring and interpreting fracture surface topography*. Cambridge University Press, Cambrige, 1999.
25. Goldstein, J. I. *et al*., *Scanning Electron Microscopy and X-Ray Microanalysis*, 2nd ed.. Plenum Press, New York, 1994.
26. Petzow, G., *Metalographic etching: Techniques for Metallography, Ceramography and Plastography*. ASM International, Ohio, 1999.
27. Inoué, S. and Spring, K. R., *Video microscopy—Fundamentals*. Plenum Press, New York, 1987.
28. Russ, J. C., *Computer assisted microscopy—The measure and analysis of images*. Plenum Press, New York, 1990.
29. Gonzalez, R. C. and Woods, R. E., *Digital image processing*, 2nd ed.. Addison-Wesley Publishing Company Inc, Reading, 1992.
30. Wojnar, L., *Image analysis: applications in materials engineering*. CRC Press, Boca Raton, 1999.
31. Russ, J. C. and DeHoff, R. T., *Practical stereology*, 2nd ed. Plenum Press, New York, 2000.
32. Chinga, G., http://rsb.info.nih.gov/ij/plugin/waveness-roughness.html.
33. Costa, L. F. and Cesar, R. M. Jr., *Shape analysis and classification*. CRC Press, Boca Raton, 2001.
34. Celli, A., Tucci, A., Esposito, L. and Palmonari, C., Fractal analysis of cracks in alumina–zirconia composites. *J. Eur. Ceram. Soc*., 2003, **23**, 469–479.
35. Mussler, B., Swain, M. V. and Claussen, N., Dependence of fracture toughness of alumina on grain size and test technique. *J. Am. Ceram. Soc*., 1982, **65**, 566–572.
36. Müller, J. W., Possible advantages of robust evaluation of comparisons. *J. Res. Natl. Stand. Technol*, 2000, **105**, 551–555.
37. Jain, A. K., *Fundamentals of digital image processing*. Prentice Hall-International, Englewood Cliffs, 1989.
38. Howard, C. V. and Reed, M. G., *Unbiased stereology: Three dimensional measurement in microscopy*. Bios Scientific Publisher, Oxford, Oxford, 1998.
39. American Society for Testing Materials. Standard test method for determining average grains size using semiautomatic and automatic image analysis. ASTM E1382-97.
40. Kurzydlowsky, K. J. and Ralph, B., *The quantitative description of microstructure of materials*. CRC Press, Boca Raton, 1995.